APPLIED PHYSICS

Full voltage manipulation of the resistance of a magnetic tunnel junction

Aitian Chen[1], Yuelei Zhao[1], Yan Wen[1], Long Pan[2], Peisen Li[2], Xi-Xiang Zhang[1]*

One of the motivations for multiferroics research is to find an energy-efficient solution to spintronic applications, such as the solely electrical control of magnetic tunnel junctions. Here, we integrate spintronics and multiferroics by depositing MgO-based magnetic tunnel junctions on ferroelectric substrate. We fabricate two pairs of electrodes on the ferroelectric substrate to generate localized strain by applying voltage. This voltage-generated localized strain has the ability to modify the magnetic anisotropy of the free layer effectively. By sequentially applying voltages to these two pairs of electrodes, we successively and unidirectionally rotate the magnetization of the free layer in the magnetic tunnel junctions to complete reversible 180° magnetization switching. Thus, we accomplish a giant nonvolatile solely electrical switchable high/low resistance in magnetic tunnel junctions at room temperature without the aid of a magnetic field. Our results are important for exploring voltage control of magnetism and low-power spintronic devices.

INTRODUCTION

The resistance of a magnetic tunnel junction (MTJ) that consists of two ferromagnetic layers sandwiching a thin nonmagnetic insulating layer depends on the angle between the magnetization of the two magnetic layers (*1*, *2*). When the two magnetizations in both ferromagnetic layers are parallel (antiparallel) to each other, the resistance of the MTJ is lowest (highest). These two states with the lowest and highest resistances can be designated as bits 0 and 1 in the magnetoresistive random access memory (MRAM) and other spintronic applications (*1*–*4*). To store binary bits 0 and 1, the parallel and antiparallel magnetization configurations need to be easily mutually switched, thus accomplishing a "writing" operation. Conventionally, the writing of bits uses a magnetic field, a spin-orbit torque (*5*–*7*), or a spin-transfer torque (STT) (*8*, *9*), each of which requires a high electric current density to be flowing in the device and consequently dissipates significant energy.

The efficient operation of MTJs with lower energy consumption becomes more important with their increasing miniaturization (*10*). Much effort has been dedicated to developing electrical approaches to manipulating MTJs, such as using electric field–modified coercivity (*11*) or magnetization precession (*12*) with the assistance of a magnetic field and using ferroelectric materials as the barrier layer with cryogenic operation temperature (*13*–*15*). The manipulation of magnetization in nanomagnets by voltage has been realized in ferromagnetic/ferroelectric multiferroic heterostructures (*16*–*18*), which is most effectively applied to manipulate MTJs with voltage instead of magnetic field or current. Therefore, integrating spintronics and multiferroics is emerging as a promising strategy for memory and logic (*19*) and presents a new opportunity for the energy-efficient operation of MTJs, the key elements in spintronics. Motivated by the successes in the electrical control of magnetism using ferromagnetic/ferroelectric multiferroic heterostructures (*20*–*23*), several groups have realized the electrical manipulation of magnetoresistance (MR) in MTJs deposited on ferroelectric substrates (*24*–*26*), in which the magnetization of the free layer is rotated by the strain transferred from the ferroelectric substrate. However, in these experiments, the magnetization in the free layer with an in-plane uniaxial anisotropy could only be rotated from one of the stable states up to 90° by the voltage-induced strain. This means that the parallel and antiparallel magnetization configurations of the MTJ cannot be switched as desired, since a 180° magnetization switching of the free layer is required. Although several schemes (*27*, *28*) have been theoretically proposed to achieve 180° magnetization switching, the experimental demonstration is still challenging (*29*) and remains elusive.

Recently, a new strategy to fully reverse the magnetization by voltage was proposed (*30*) and experimentally demonstrated in nanomagnets with uniaxial anisotropy (*31*). In this approach, two pairs of electrodes with a special arrangement (*30*), in which the joint lines of the paired electrodes are noncollinear with the easy axis of the nanomagnet by ±30°, are used to apply the voltage sequentially. In this configuration, once one pair of electrodes has been activated by a voltage, the magnetization of the nanomagnet is rotated from one stable state by an acute angle. With the activation of another set of paired electrodes, the magnetization is rotated closer to another stable state. After turning off the voltage, the magnetization aligns toward the other stable state, accomplishing a full 180° magnetization reversal from the initial direction through two steps of rotations. Therefore, by programming the activation of two paired electrodes, the magnetization direction in the nanomagnets can be reversed reproducibly (*31*). If this strategy is applied to an MTJ to reverse the magnetization in the free layer, then we can write bits with low energy dissipation and low write error probability (*30*, *32*).

Here, we report full voltage manipulation of the resistance of an MTJ without the assistance of a magnetic field. We deposit high-quality MgO-based MTJs on $Pb(Mg_{1/3}Nb_{2/3})_{0.7}Ti_{0.3}O_3$ (PMN-PT) ferroelectric substrate and fabricate two pairs of electrodes that are activated by voltage to generate localized strain. By sequentially applying the voltage to the two electrode pairs, we demonstrate that it is feasible to control the resistance in MTJs with voltage between high and low nonvolatile resistance states via reversing the magnetization of the free layer. This is a well-recognized energy-efficient strategy for "writing bit" in MRAM. Therefore, our work represents a crucial step toward the ultralow-power operation of MRAM.

[1]Physical Science and Engineering Division, King Abdullah University of Science and Technology, Thuwal 23955-6900, Saudi Arabia. [2]College of Intelligence Science and Technology, National University of Defense Technology, Changsha 410073, China. *Corresponding author. Email: xixiang.zhang@kaust.edu.sa

RESULTS

The effect of voltage-induced localized strain on MTJs

Figure 1A shows a schematic diagram of the experiment. The voltage was applied between one pair of shorted electrodes (AA) and the PMN-PT ferroelectric substrate, and an MTJ was placed at the center of the electrodes. It is notable that the voltage was not directly applied to the MTJ device to avoid the potential damage to the MTJs. The MTJ was etched into an elliptical shape of $18 \times 6\ \mu m^2$ to give the free layer an in-plane uniaxial anisotropy along its major axis. In this arrangement, the major axis or the uniaxial easy axis was perpendicular to the joint line of the AA electrodes. The detailed MTJ stack is illustrated in Fig. 1B, in which the CoFeB layer below the MgO layer is pinned by the antiferromagnetic IrMn layer and the CoFeB layer above the MgO layer is the free layer to be rotated by voltage through strain-mediated magnetoelectric coupling. As reported, a localized strain was generated upon application of a voltage to the shorted electrode pair and the grounded substrate (*31*, *33*). To confirm this, we also simulated the distribution of the localized strain using finite element analysis (fig. S1). Figure 1C shows the distribution of localized tensile strain ε_{yy}-ε_{xx} between the two electrodes under a positive voltage of 400 V, as extracted from simulation. To obtain enough piezostrain to modify the magnetic easy axis of the CoFeB ferromagnetic layer via inverse magnetostriction effect, these large voltages (usually several hundred volts) are needed because of the thick ferroelectric substrate. It is clear that a nearly uniform localized tensile strain along the joint line of the electrodes was generated. This uniform localized strain is different from that generated by one electrode scheme (*34*, *35*), where the piezostrain is governed by the intrinsic anisotropy of piezoelectric coefficients, and consequently, its orientation is always fixed in a certain crystal orientation (*35*, *36*). Furthermore, this anisotropic strain generated with one electrode is nonuniform at the microscale (*16*) and difficult to control, which leads to different magnetization responses to the electric field in magnetic disks (*16*–*18*, *37*) that are fabricated on a ferroelectric substrate with complex ferroelectric domain structures. Unlike a single-electrode approach that generates a nonuniform strain, the pair of shorted electrodes generates a strong and uniform strain between the two electrodes with a fixed direction (along the joint line of the two electrodes) and controllable strength, which can manipulate individual magnetic disks within the gap between the two electrodes and enables the application of arrays of indexed magnetic disks (*33*). Moreover, this anisotropic strain generated by the use of one electrode pair is available and universal for ferroelectric material, regardless if it is single crystal (*26*, *31*) or polycrystalline (*33*). Therefore, this voltage-induced uniform localized strain is superior for application in small devices, such as MTJs with a microscale or even nanoscale size.

To explore how the voltage-induced localized strain manipulates the resistance of MTJs, we measured the MR curves at room temperature with in situ voltages, as shown in Fig. 1D. The MR curve at 0 V has a well-defined narrow and square hysteresis with a large tunnel MR (TMR) ratio [TMR = $(R_{high} - R_{low})/R_{low} \approx 208\%$], indicating the high quality of the MTJ. It is evident that under an applied voltage of 400 V, the curve is gradual, which is notably different to the curve without voltage. The results shown in Fig. 1D, which are consistent with those of previous work (*24*, *25*), indicate that the voltage-generated strain rotates the magnetization of the free layer (fig. S2), but not the magnetization of the pinned layer in the defined magnetic field range.

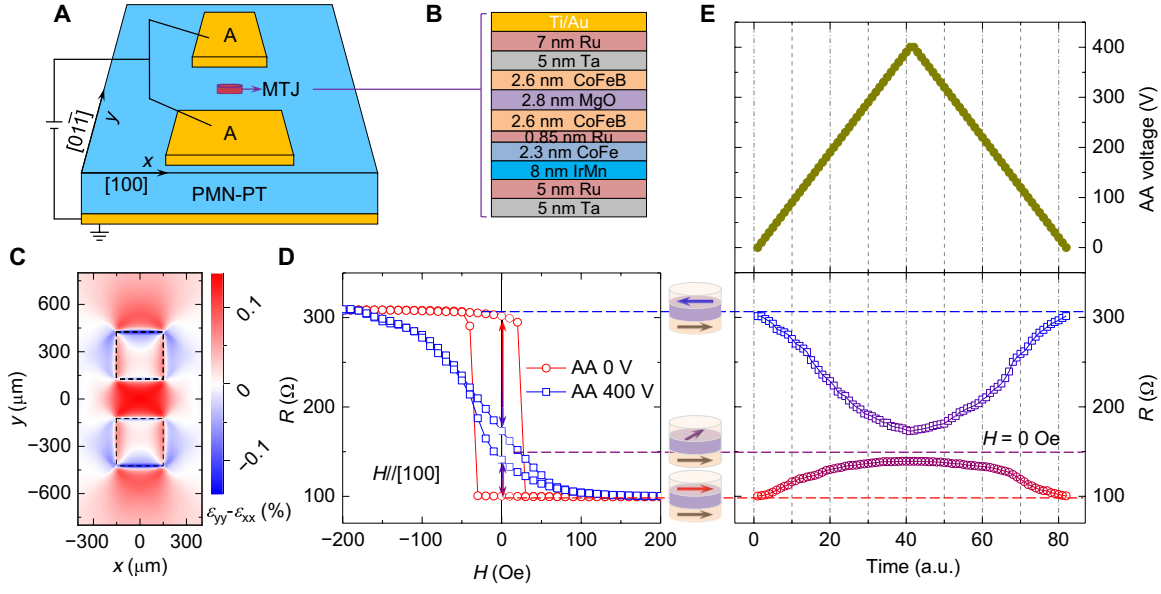

Fig. 1. Voltage manipulation of the MTJ by one pair of electrodes. (**A**) Schematic of the experimental setup. One pair of AA electrodes was deposited on the PMN-PT, and an elliptical MTJ device of $18 \times 6\ \mu m^2$ was placed at the center of the gap. Voltage was applied to the AA electrodes to generate localized strain, and the bottom of the substrate was grounded. (**B**) The detailed structure of the MgO-based MTJ device. To enhance the performance of the devices, we used both the antiferromagnetic layer IrMn and the artificial antiferromagnetic structure of CoFe/Ru/CoFeB. With this particular design, at zero magnetic field, the top CoFeB layer acts as a free layer whose magnetization can be tuned by voltage, whereas the magnetization of the bottom CoFeB layer is fixed because of the pinning effect of the antiferromagnetic IrMn layer. (**C**) Simulated anisotropic strain distribution upon applying 400 V to the AA electrodes using finite element analysis. A uniform localized tensile strain along the *y* direction was generated at the central gap of the electrode pair. The dashed-line boxes illustrate the locations of the electrodes. (**D**) MR curves with 0 and 400 V applied at the AA electrodes. (**E**) Dependence of resistance on voltage applied to the AA electrodes under $H = 0$ Oe. The dashed lines denote the various magnetization configurations of the MTJ, as illustrated by the insets, i.e., antiparallel (red), perpendicular (purple), and parallel (blue). a.u., arbitrary units.

To further study the response of the resistance of the MTJs on the applied voltage, we measured the resistance of an MTJ as a function of voltage applied on AA electrodes at zero magnetic field, as shown in Fig. 1E. It is evident that two curves in the bottom panel of Fig. 1E correspond to two different initial states at 0 V, i.e., the high-resistance (antiparallel magnetization configuration) and low-resistance (parallel magnetization configuration) states at $H = 0$ Oe. For the initial state with high resistance at 0 V, the resistance decreased as the voltage applied to the AA electrodes increased, due to the magnetization in the free layer rotating away from the antiparallel configuration to the perpendicular configuration driven by the voltage-generated strain, although a perfect perpendicular configuration was not yet reached at 400 V. By decreasing the voltage from 400 to 0 V, the resistance returned back to the same value as that of the initial state, indicating that the magnetization of the free layer recovers its antiparallel state with the magnetization of the pinned layer and exhibits a characteristic feature of volatility. Similarly, we also observed a volatile manipulation of the resistance in MTJs for the initial state with low resistance at 0 V, as denoted by the red curve in the bottom panel of Fig. 1E. We therefore produced the following results using only one pair of electrodes: (i) We were able to rotate the magnetization of the free layer in the MTJs deposited on the ferroelectric PMN-PT substrate; (ii) however, we could only rotate the magnetization at a maximum less than 90°; (iii) after turning off the voltage, the magnetization returned back to its initial state; (iv) therefore, with one pair of electrodes, we could not realize a full magnetization reversal as desired. That is, we were unable to realize a writing bit operation precisely in the MRAM devices or other spintronic devices that require the high- and low-resistance states of MTJs to be precisely controlled (*2*, *4*).

The voltage-tuned magnetic anisotropy of the CoFeB layer using two electrode pairs

To realize the fully electrical control of MTJs, i.e., the voltage-induced 180° magnetization reversal of the free layer, we added another pair of electrodes (BB) in the direction away from the major axis by 45°, as shown in Fig. 2A. We also simulated the voltage-induced strain of the BB electrodes by finite element analysis (fig. S3). Applying a positive (or negative) voltage to the shorted BB electrodes generated a localized tensile (or compressive) strain along the joint line of the electrodes at the central gap. We then investigated the effect of the voltage-induced strains produced by the two electrode pairs (AA and BB) on the magnetic anisotropy of the free layer in the MTJs. Since we had demonstrated that the free layer in MTJs can be manipulated by voltage-induced strains, to simplify the fabrication process, we used a single ferromagnetic layer deposited on the PMN-PT substrate with the detailed structure of PMN-PT/Ta (5 nm)/Ru (5 nm)/CoFeB (5 nm)/Ta (5 nm) for the study. The variation of the magnetic property of this CoFeB sample was studied using the magneto-optical Kerr effect (MOKE) with in situ voltages, and the magnetic anisotropy was obtained by measuring the angular dependence of the magnetic hysteresis loops.

In multiferroic heterostructures integrating ferroelectric and magnetic materials, the piezostrain ε generated in ferroelectric materials by applying voltage transfers to the magnetic material, resulting in a magnetic anisotropy $E = \frac{3}{2}\lambda Y\varepsilon$ due to the converse magnetostriction effect (*21*, *25*), where λ and Y are the magnetostriction coefficient and Young's modulus of magnetic materials, respectively. Therefore, the magnetic properties of the magnetic materials can be modified through the strain-mediated magnetoelectric coupling. Figure 2 (B to E) shows the angular dependence of the remanence ratio (M_R/M_S) under different voltages applied to either the AA or BB electrodes. At 0 V, Fig. 2B demonstrates that the magnetic easy axis is along the [100] direction with the largest M_R/M_S. When a voltage of 200 V was applied to the BB electrodes, a tensile strain was generated along the joint line of the BB electrodes (fig. S3B). This tensile strain induced a uniaxial magnetic anisotropy with an easy axis along the joint line of the BB electrodes, due to the positive magnetostriction coefficient of the CoFeB film (*24*, *38*), so that the easy axis was rotated away from the [100] direction by about 45°, which is evidenced by the data shown in Fig. 2C. When a voltage of 400 V was applied to the AA electrodes, the uniaxial magnetic easy axis was altered to be aligned with the [01$\bar{1}$] direction of the substrate or y axis (Fig. 2D) because of the voltage-induced tensile strain along the [01$\bar{1}$] direction (Fig. 1B). To successively control the magnetic easy axis by voltage, we applied a negative voltage of −200 V to the BB electrodes rather than a positive 200 V. It is clear that the easy axis was rotated to a direction that was nearly perpendicular to the joint line of the BB electrodes (Fig. 2E), because the voltage-induced compressive strain along the joint line of the BB electrodes (fig. S3C) induces a uniaxial magnetic anisotropy perpendicular to the joint line of the BB electrodes. Therefore, the results shown in Fig. 2 demonstrate that voltage-induced localized strains enabled us to successively rotate the easy axis of the ferromagnetic film via strain-mediated magnetoelectric coupling. On the basis of the experiments described above, we can conclude that the successive rotation of the magnetic easy axis can be realized by programming the application of voltage to two pairs of electrodes and that voltage-driven reversible 180° magnetization switching can, thus, be achieved.

Voltage-driven fully reversible 180° magnetization switching

We performed micromagnetic simulations to investigate how voltage-driven reversible 180° magnetization switching could be achieved. We set a single domain along the [100] direction (the $+x$ direction in the x-y plane) of the PMN-PT substrate (the pinning direction of the MTJs) as the initial state (Fig. 3A). When applying a voltage of 200 V to the BB electrodes, the magnetic moment **M** rotated to the induced magnetic easy axis, which was away from the x direction by an acute angle of 45° (Fig. 3B). Next, by applying 400 V to the AA electrodes and then removing the voltage on the BB electrodes, **M** reoriented to the $-y$ direction as illustrated in Fig. 3C because the magnetic easy axis induced by the tensile strain was along the y axis (Fig. 2D). Subsequently, the application of −200 V to the BB electrodes drove **M** to rotate unidirectionally by another 45° (Fig. 3D). Last, **M** rotated to the $-x$ direction after the voltage was removed, as shown in Fig. 3E, since the $-x$ direction is another stable state of **M** at 0 V. Through applying the above sequential voltages to AA and BB electrodes (i.e., 0 V → BB 200 V → AA 400 V → BB −200 V → 0 V), the **M** completed a 180° reversal by successive clockwise 45° rotations (Fig. 3, A to E). Similarly, the **M** could be reverted back to its initial state after another 180° rotation by applying the same sequential voltages, as shown in Fig. 3, E to H. Note that a 180° magnetization switching can also be accomplished by implementing sequential voltages of 0 V → BB −200 V → AA 400 V → BB 200 V → 0 V, through successive anticlockwise 45° rotations. Here, the role of the BB electrodes was to break the symmetry and to drive **M** to rotate unidirectionally. It is therefore evident that a reversible and nonvolatile

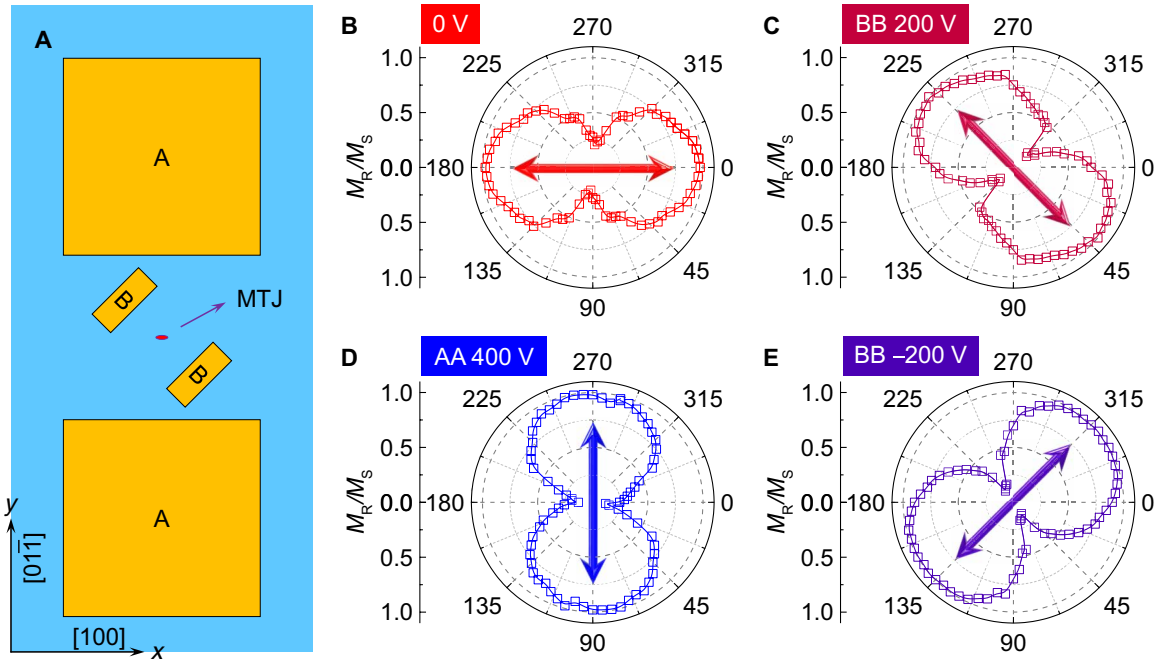

Fig. 2. Tuning the magnetic anisotropy of the free layer by voltage using two pairs of electrodes. (**A**) Schematic top view of the sample structure with two pairs of AA and BB electrodes. An elliptical MTJ device of 18 × 6 μm^2 was placed at the center of two electrode pairs. The major axis of the elliptical device was along the *x* axis. The pinning direction of the MTJ was along the [100] direction of the PMN-PT substrate (+*x* axis). The joint line of the AA electrodes was perpendicular to the pinning direction, while that of the BB electrodes deviated from the pinning direction by 45°. (**B** to **E**) Polar curves of the angular-dependent M_R/M_S of a CoFeB layer, when the applied voltages were 0 V (B), BB 200 V (C), AA 400 V (D), and BB −200 V (E). The [100] direction of the PMN-PT substrate was defined as 0°. The double-headed arrows indicate the direction of the magnetic easy axis.

manipulation of 180° magnetization reversal can be realized by synergistically applying voltages to AA and BB electrode pairs via successive unidirectional 45° magnetization rotations, which is essential to realizing the fully electrical control of MTJs.

Full control of MTJs solely by voltage

It is well documented that the resistance of MTJs depends on the relative magnetization orientation of the free layer and the pinned layer. In our devices (Fig. 1C), at zero magnetic field, the magnetization of the pinned layer was fixed, while the magnetization of the free layer could be modulated by voltage (*24*, *25*). The resistance of MTJs at $H = 0$ Oe is, thus, able to reveal the magnetization rotation of the free layer driven by voltage. Figure 3I shows the dependence of the resistance of MTJ on voltage at zero magnetic field to demonstrate the aforementioned voltage-driven 180° magnetization switching in Fig. 3 (A to H). In contrast to the results shown in Fig. 1E, in which only AA electrodes were used, both AA and BB electrode pairs worked synergistically in Fig. 3I (fig. S4). The resistance of the MTJ started to increase from the low-resistance state at 0 V (parallel magnetization configuration) with the increasing positive voltage applied to the BB electrodes, since the magnetization of the free layer deviated from the magnetization direction of the pinned layer. After applying 400 V to the AA electrodes and removing the voltage on the BB electrodes, the magnetization of the free layer was approximately perpendicular to that of the pinned layer, a rotation of nearly 90° for the magnetization in the free layer. Furthermore, the application of negative voltage to the BB electrodes drove the magnetization of the free layer to rotate by more than 90°, as indicated by the continuous increase in resistance. With continuous application of the voltages to AA and BB electrodes sequentially, the magnetization of the free layer lastly became antiparallel to that of the pinned layer. Consequently, the resistance of the MTJ eventually approached the high-resistance state, as represented in Fig. 3I. Moreover, the high-resistance state could also be switched to the low-resistance state by operating the same sequential voltages (i.e., 0 V → BB 200 V → AA 400 V → BB −200 V → 0 V). This high-/low-resistance switching is stable, reversible, and nonvolatile, as shaded in pink and blue in Fig. 3I. The switchable high/low resistance suggests a reversible and nonvolatile 180° magnetization switching, which is consistent with the simulations shown in Fig. 3 (A to H). These results are distinct from those in Fig. 1E and previous work (*24*–*26*), where the rotation of magnetization is limited to 90°. Thus, full control of MTJs, deriving from the voltage-switched magnetization of the free layer by 180°, is realized at zero magnetic field by synergistically applying voltages to the AA and BB electrodes.

The emerging electrical control of MTJs is drawing much attraction for its minimal power dissipation. Most of the energy consumed in our devices is that which was dissipated to activate the electrodes to produce localized strain (*31*). The energy consumption per unit area can be estimated by CV^2/A (*24*, *30*, *39*), where C, V, and A denote the capacitance of the ferroelectric layer, the applied voltage, and the area of the device, respectively. The capacitance can be written as $C = \varepsilon_r\varepsilon_0 A/d$ (*31*), assuming a parallel plate capacitor (A is the area of the electrode, d is the thickness of the ferroelectric layer, ε_r is the relative dielectric constant of the ferroelectric layer, and ε_0 is the vacuum dielectric constant). Thus, the energy consumption per unit area can be expressed as $\varepsilon_r\varepsilon_0 V^2/d$. In our devices, the thickness and ε_r of PMN-PT substrate were approximately 500 μm and 3000 (*40*),

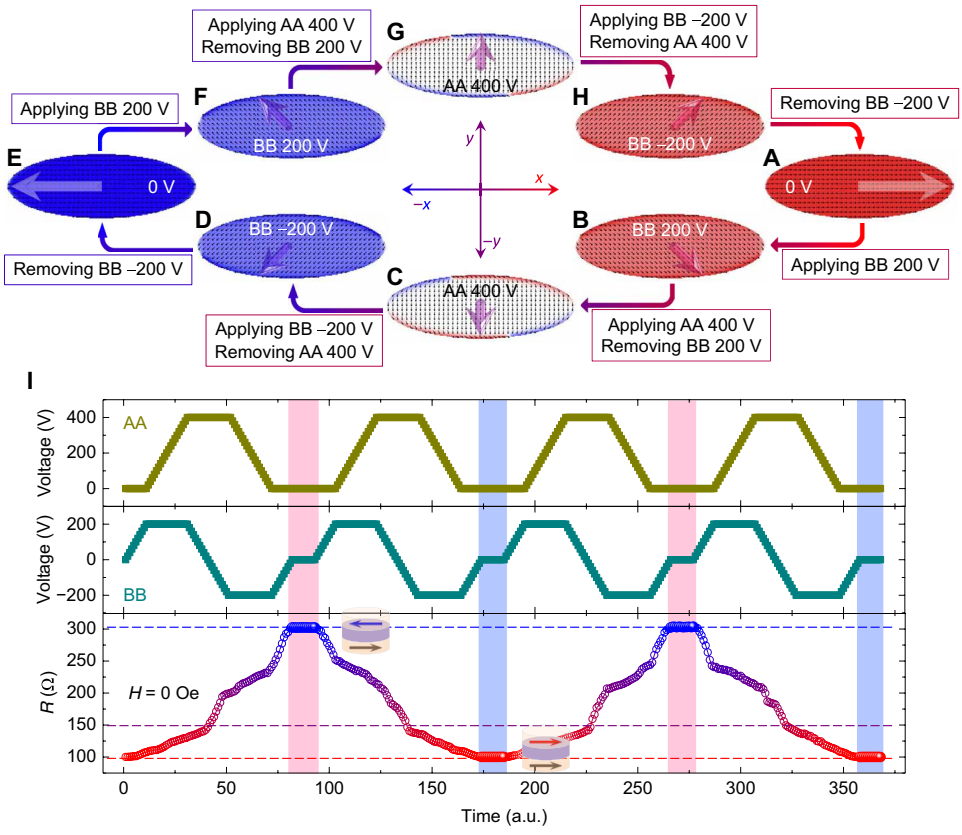

Fig. 3. Reversible and nonvolatile full control of MTJs by voltage-driven 180° magnetization switching. (**A** to **H**) Simulated magnetization profiles of the free layer at various voltages applied to the AA and BB electrode pairs. A 180° magnetization switching was accomplished by implementing sequential voltages of 0 V (A) → BB 200 V (B) → AA 400 V (C) → BB −200 V (D) → 0 V (E) via successive unidirectional 45° rotations, and the **M** reverted back to the initial state after the same sequential voltages were implemented (E to H), suggesting reversibility and nonvolatility. The arrows schematically indicate the magnetization directions of the free layer. (**I**) Dependence of the resistance of an MTJ on voltage synergistically applied to the AA and BB electrode pairs at $H = 0$ Oe. The reversible resistance switching between high- and low-resistance states corresponds to the antiparallel and parallel magnetization configurations of the MTJ, as illustrated by the insets, which indicates the 180° magnetization switching of the free layer driven by voltage. The red, purple, and blue dashed lines denote the antiparallel, perpendicular, and parallel magnetization configurations of the MTJ, respectively. The stable resistance states with a giant modulation of approximately 200%, highlighted by the vertical pink and blue shaded lines, demonstrate that this 180° magnetization switching and full control of MTJs by voltage are reversible and nonvolatile.

respectively. The energy consumption per unit area was therefore approximately 0.85 mJ cm^{-2} for a 400-V operation voltage, and 0.21 mJ cm^{-2} for 200 V; thus, the energy dissipation for write operation is approximately 1.06 mJ cm^{-2} by applying 400 V to the AA electrodes and applying 200 V to the BB electrodes, while the energy dissipation in state-of-the-art STT MTJs is about 3 to 4 mJ cm^{-2} (*29*), which is larger than the dissipation in our devices. The energy consumption per bit for a circular-shaped MTJ of 100 nm in diameter is about 85 fJ bit^{-1} for a 400-V operation voltage and about 21 fJ bit^{-1} for 200 V, which is comparable with that of STT MTJs (about 100 fJ bit^{-1}) (*41*, *42*). Although the present applied voltage is high for practical applications because of the thick PMN-PT substrate, the voltage can be further reduced to less than several volts using PMN-PT thin film (*43*). In addition, the energy consumption per bit can be further reduced using ferroelectric film, even as low as 0.16 fJ bit^{-1} (*44*), owing to the lower operation voltage. Moreover, using ferroelectric film can shrink the size of the electrodes and also their distance. Recently, high-quality PMN-PT epitaxial thin films on Si wafers with giant piezoelectricity have been reported to enable low voltage control of magnetization rotation (*43*), which offers a promising approach to integrating the MTJs/ferroelectric structure with current silicon-based electronics. Thus, this fully electrical manipulation of MTJs can be realized using ferroelectric film with low voltage and ultralow-power dissipation, and our present work based on PMN-PT substrate gives a prelude to this attractive future application.

DISCUSSION

We have experimentally demonstrated a room temperature giant (about 200%), reversible, and nonvolatile fully electrical control of MTJs deposited on ferroelectric substrate at zero magnetic field. This fully electrical control of MTJs was ascribed to the voltage-rotated magnetization of the free layer, which was achieved by sequentially activating two pairs of electrodes, via strain-mediated magnetoelectric coupling. The voltage-driven successive unidirectional magnetization rotation led to 180° magnetization switching of the free layer, such that the magnetization configuration of the MTJs could be switched between antiparallel and parallel, as revealed by the full control of MTJs. The full control of MTJs solely by voltage represents a crucial step toward electrical-driven spintronic devices with ultralow-power consumption. It is notable that the introduction of two pairs of electrodes in our device enabled low-power

switching of MTJs at the expense of memory density. Therefore, these full voltage-controlled MTJs are most attractive for energy-efficient applications, such as wearable electronics (*45*) and implantable medical devices (*46*), where low-power consumption is a major consideration.

MATERIALS AND METHODS

Sample fabrication

The MTJ multilayer films from the substrate side consisted of Ta (5 nm)/Ru (5 nm)/IrMn (8 nm)/CoFe (2.3 nm)/Ru (0.85 nm) CoFeB (2.6 nm)/MgO (2.8 nm)/CoFeB (2.6 nm)/Ta (5 nm)/Ru (7 nm) and were deposited on PMN-PT (011) single crystals with a size of $10 \times 10 \times 0.5$ mm^3. The films were processed into an elliptical shape of 18×6 μm^2 by photolithography and ion milling. The major axis was along the [100] crystal direction of the PMN-PT substrate. Subsequently, the MTJ devices were annealed in a vacuum at 360°C for 2 hours with a magnetic field of 8000 Oe along the major axis of the elliptical MTJ pillar to crystallize CoFeB/MgO/CoFeB structures and to improve the TMR ratio. To study the effect of the voltage-induced localized strain on the magnetic anisotropy of the CoFeB free layer, a single CoFeB film was sputtered on PMN-PT (011) with the structure of PMN-PT/Ta (5 nm)/Ru (5 nm)/CoFeB (5 nm)/Ta (5 nm). The CoFe, CoFeB, and IrMn denote $Co_{70}Fe_{30}$, $Co_{40}Fe_{40}B_{20}$, and $Ir_{20}Mn_{80}$ alloys with nominal target compositions, respectively. All of the stack structures in this study were deposited using a Singulus sputtering system at room temperature with a base vacuum of 1×10^{-6} Pa. The patterned electrodes, Ti (10 nm) and Au (50 nm), were fabricated using lift-off. The size of the AA electrodes was 300×300 μm^2 with a distance of 250 μm between the facing edges, and the joint line of the AA electrodes was perpendicular to the major axis, i.e., the pinning direction of the MTJs. The size of the BB electrodes was 100×40 μm^2 with a distance of 120 μm, and the joint line of the BB electrodes was away from the major axis of the MTJs by 45°. Ti (10 nm) and Au (150 nm) layers were sputtered on the bottom of PMN-PT as bottom electrode.

Magnetic and magnetotransport measurements

The magnetic anisotropy of the CoFeB film was performed using Durham NanoMOKE 2 with in situ voltages. The resistance of the MTJs was measured by a homemade electromagnet system, using the four-probe method with a Keithley 6221 current source and a Keithley 2182 nanovolt meter. The applied voltage was generated by a Keithley 6517 electrometer. All of the measurements were conducted at room temperature.

Simulations of voltage-induced localized strains

The voltage-induced localized strains were simulated by finite element analysis (COMSOL Multiphysics package). The piezoelectric coefficients of the PMN-PT (011) were taken from (*47*). The simulated substrate was 5000×5000 μm^3, which was large enough to estimate the voltage-induced localized strains.

Micromagnetic simulations on the magnetization evolution

Micromagnetic simulation was performed using the object-oriented micromagnetic framework (OOMMF) software to study the magnetization evolution of the free layer under voltages. Similar to the device structure, an elliptical-shaped CoFeB disk of 18×6 μm^2 was built and discretized in the computational cells of 10 nm × 10 nm. The saturation magnetization, M_S, was 1200 emu cm^{-3}, and the uniform exchange constant, A, was 2.8×10^{-11} J m^{-1} (*37*). To simulate the domain structures of the free layer of the MTJ under voltages, a single domain along the [100] direction of PMN-PT (the pinning direction of the MTJs) was set as the initial state. The magnetic anisotropy constants under different voltages were obtained from the M-H loops that were measured by MOKE (Fig. 2) using the area method (*48*).

SUPPLEMENTARY MATERIALS

Supplementary material for this article is available at http://advances.sciencemag.org/cgi/content/full/5/12/eaay5141/DC1

Fig. S1. The localized strain induced by a voltage of 400 V applied on shorted AA electrodes.
Fig. S2. Modulating the magnetic property of the CoFeB layer by voltage-induced localized strain using electrode pair AA.
Fig. S3. The voltage-induced localized strain by activating the BB electrodes.
Fig. S4. Optical image of an MTJ cell with two pairs of AA and BB electrodes.

REFERENCES AND NOTES

1. S. A. Wolf, D. D. Awschalom, R. A. Buhrman, J. M. Daughton, S. von Molnar, M. L. Roukes, A. Y. Chtchelkanova, D. M. Treger, Spintronics: A spin-based electronics vision for the future. *Science* **294**, 1488–1495 (2001).
2. C. Chappert, A. Fert, F. N. Van Dau, The emergence of spin electronics in data storage. *Nat. Mater.* **6**, 813–823 (2007).
3. S. Tehrani, J. M. Slaughter, M. Deherrera, B. N. Engel, N. D. Rizzo, J. Salter, M. Durlam, R. W. Dave, J. Janesky, B. Butcher, K. Smith, G. Grynkewich, Magnetoresistive random access memory using magnetic tunnel junctions. *Proc. IEEE* **91**, 703–714 (2003).
4. S. Bhatti, R. Sbiaa, A. Hirohata, H. Ohno, S. Fukami, S. N. Piramanayagam, Spintronics based random access memory: A review. *Mater. Today* **20**, 530–548 (2017).
5. L. Liu, C. Pai, Y. Li, H. W. Tseng, D. C. Ralph, R. A. Buhrman, Spin-torque switching with the giant spin Hall effect of tantalum. *Science* **336**, 555–558 (2012).
6. N. Sato, F. Xue, R. M. White, C. Bi, S. X. Wang, Two-terminal spin-orbit torque magnetoresistive random access memory. *Nat. Electron.* **1**, 508–511 (2018).
7. M. Wang, W. Cai, D. Zhu, Z. Wang, J. Kan, Z. Zhao, K. Cao, Z. Wang, Y. Zhang, T. Zhang, C. Park, J. Wang, A. Fert, W. Zhao, Field-free switching of a perpendicular magnetic tunnel junction through the interplay of spin-orbit and spin-transfer torques. *Nat. Electron.* **1**, 582–588 (2018).
8. A. Brataas, A. D. Kent, H. Ohno, Current-induced torques in magnetic materials. *Nat. Mater.* **11**, 372–381 (2012).
9. S. Ikeda, K. Miura, H. Yamamoto, K. Mizunuma, H. D. Gan, M. Endo, S. Kanai, J. Hayakawa, F. Matsukura, H. Ohno, A perpendicular-anisotropy CoFeB-MgO magnetic tunnel junction. *Nat. Mater.* **9**, 721–724 (2010).
10. D. Sander, S. O. Valenzuela, D. Makarov, C. H. Marrows, E. E. Fullerton, P. Fischer, J. McCord, P. Vavassori, S. Mangin, P. Pirro, B. Hillebrands, A. D. Kent, T. Jungwirth, O. Gutfleisch, C. G. Kim, A. Berger, The 2017 magnetism roadmap. *J. Phys. D Appl. Phys.* **50**, 363001 (2017).
11. W.-G. Wang, M. Li, S. Hageman, C. L. Chien, Electric-field-assisted switching in magnetic tunnel junctions. *Nat. Mater.* **11**, 64–68 (2012).
12. Y. Shiota, T. Nozaki, F. Bonell, S. Murakami, T. Shinjo, Y. Suzuki, Induction of coherent magnetization switching in a few atomic layers of FeCo using voltage pulses. *Nat. Mater.* **11**, 39–43 (2012).
13. D. Pantel, S. Goetze, D. Hesse, M. Alexe, Reversible electrical switching of spin polarization in multiferroic tunnel junctions. *Nat. Mater.* **11**, 289–293 (2012).
14. V. Garcia, M. Bibes, L. Bocher, S. Valencia, F. Kronast, A. Crassous, X. Moya, S. Enouz-Vedrenne, A. Gloter, D. Imhoff, C. Deranlot, N. D. Mathur, S. Fusil, K. Bouzehouane, A. Barthelemy, Ferroelectric control of spin polarization. *Science* **327**, 1106–1110 (2010).
15. M. Gajek, M. Bibes, S. Fusil, K. Bouzehouane, J. Fontcuberta, A. Barthelemy, A. Fert, Tunnel junctions with multiferroic barriers. *Nat. Mater.* **6**, 296–302 (2007).
16. R. Lo Conte, Z. Xiao, C. Chen, C. V. Stan, J. Gorchon, A. El-Ghazaly, M. E. Nowakowski, H. Sohn, A. Pattabi, A. Scholl, N. Tamura, A. Sepulveda, G. P. Carman, R. N. Candler, J. Bokor, Influence of nonuniform micron-scale strain distributions on the electrical reorientation of magnetic microstructures in a composite multiferroic heterostructure. *Nano Lett.* **18**, 1952–1961 (2018).
17. Y. Ba, Y. Liu, P. Li, L. Wu, J. Unguris, D. T. Pierce, D. Yang, C. Feng, Y. Zhang, H. Wu, D. Li, Y. Chang, J. Zhang, X. Han, J. Cai, C. Nan, Y. Zhao, Spatially resolved electric-field manipulation of magnetism for CoFeB mesoscopic discs on ferroelectrics. *Adv. Funct. Mater.* **28**, 1706448 (2018).
18. M. Buzzi, R. V. Chopdekar, J. L. Hockel, A. Bur, T. Wu, N. Pilet, P. Warnicke, G. P. Carman, L. J. Heyderman, F. Nolting, Single domain spin manipulation by electric fields in strain coupled artificial multiferroic nanostructures. *Phys. Rev. Lett.* **111**, 027204 (2013).

19. S. Manipatruni, D. E. Nikonov, I. A. Young, Beyond CMOS computing with spin and polarization. *Nat. Phys.* **14**, 338–343 (2018).
20. J. Hu, L. Chen, C. Nan, Multiferroic heterostructures integrating ferroelectric and magnetic materials. *Adv. Mater.* **28**, 15–39 (2016).
21. A. T. Chen, Y. G. Zhao, Electrical manipulation of magnetism through strain-mediated magnetoelectric coupling in multiferroic heterostructures. *APL Mater.* **4**, 032303 (2016).
22. C. A. F. Vaz, Electric field control of magnetism in multiferroic heterostructures. *J. Phys. Condens. Matter* **24**, 333201 (2012).
23. N. X. Sun, G. Srinivasan, Voltage control of magnetism in multiferroic heterostructures and devices. *Spine* **2**, 1240004 (2012).
24. A. Chen, Y. Wen, B. Fang, Y. Zhao, Q. Zhang, Y. Chang, P. Li, H. Wu, H. Huang, Y. Lu, Z. Zeng, J. Cai, X. Han, T. Wu, X. Zhang, Y. Zhao, Giant nonvolatile manipulation of magnetoresistance in magnetic tunnel junctions by electric fields via magnetoelectric coupling. *Nat. Commun.* **10**, 243 (2019).
25. P. Li, A. Chen, D. Li, Y. Zhao, S. Zhang, L. Yang, Y. Liu, M. Zhu, H. Zhang, X. Han, Electric field manipulation of magnetization rotation and tunneling magnetoresistance of magnetic tunnel junctions at room temperature. *Adv. Mater.* **26**, 4320–4325 (2014).
26. Z. Zhao, M. Jamali, N. D'Souza, D. Zhang, S. Bandyopadhyay, J. Atulasimha, J. Wang, Giant voltage manipulation of MgO-based magnetic tunnel junctions via localized anisotropic strain: A potential pathway to ultra-energy-efficient memory technology. *Appl. Phys. Lett.* **109**, 092403 (2016).
27. R. Peng, J. J. Wang, J. Hu, L. Chen, C. Nan, Electric-field-driven magnetization reversal in square-shaped nanomagnet-based multiferroic heterostructure. *Appl. Phys. Lett.* **106**, 142901 (2015).
28. J. J. Wang, J. M. Hu, J. Ma, J. X. Zhang, L. Q. Chen, C. W. Nan, Full 180° magnetization reversal with electric fields. *Sci. Rep.* **4**, 7507 (2014).
29. J. T. Heron, J. L. Bosse, Q. He, Y. Gao, M. Trassin, L. Ye, J. D. Clarkson, C. Wang, J. Liu, S. Salahuddin, D. C. Ralph, D. G. Schlom, J. Iniguez, B. D. Huey, R. Ramesh, Deterministic switching of ferromagnetism at room temperature using an electric field. *Nature* **516**, 370–373 (2014).
30. A. K. Biswas, S. Bandyopadhyay, J. Atulasimha, Complete magnetization reversal in a magnetostrictive nanomagnet with voltage-generated stress: A reliable energy-efficient non-volatile magneto-elastic memory. *Appl. Phys. Lett.* **105**, 072408 (2014).
31. A. K. Biswas, H. Ahmad, J. Atulasimha, S. Bandyopadhyay, Experimental demonstration of complete 180° reversal of magnetization in isolated Co nanomagnets on a PMN-PT substrate with voltage generated strain. *Nano Lett.* **17**, 3478–3484 (2017).
32. A. K. Biswas, J. Atulasimha, S. Bandyopadhyay, An error-resilient non-volatile magneto-elastic universal logic gate with ultralow energy-delay product. *Sci. Rep.* **4**, 7553 (2014).
33. J. Cui, J. L. Hockel, P. K. Nordeen, D. M. Pisani, C. Liang, G. P. Carman, C. S. Lynch, A method to control magnetism in individual strain-mediated magnetoelectric islands. *Appl. Phys. Lett.* **103**, 232905 (2013).
34. T. Wu, A. Bur, P. Zhao, K. P. Mohanchandra, K. Wong, K. L. Wang, C. S. Lynch, G. P. Carman, Giant electric-field-induced reversible and permanent magnetization reorientation on magnetoelectric Ni/(011) $[Pb(Mg_{1/3}Nb_{2/3})O_3]_{(1-x)}$-$[PbTiO_3]_x$ heterostructure. *Appl. Phys. Lett.* **98**, 012504 (2011).
35. L. Yang, Y. Zhao, S. Zhang, P. Li, Y. Gao, Y. Yang, H. Huang, P. Miao, Y. Liu, A. Chen, C. W. Nan, C. Gao, Bipolar loop-like non-volatile strain in the (001)-oriented $Pb(Mg_{1/3}Nb_{2/3})O_3$-$PbTiO_3$ single crystals. *Sci. Rep.* **4**, 4591 (2014).
36. S. E. Park, T. R. Shrout, Ultrahigh strain and piezoelectric behavior in relaxor based ferroelectric single crystals. *J. Appl. Phys.* **82**, 1804–1811 (1997).
37. P. Li, Y. Zhao, S. Zhang, A. Chen, D. Li, J. Ma, Y. Liu, D. T. Pierce, J. Unguris, H. Piao, H. Zhang, M. Zhu, X. Zhang, X. Han, M. Pan, C. Nan, Spatially resolved ferroelectric domain-switching-controlled magnetism in $Co_{40}Fe_{40}B_{20}$/$Pb(Mg_{1/3}Nb_{2/3})_{0.7}Ti_{0.3}O_3$ multiferroic heterostructure. *ACS Appl. Mater. Interfaces* **9**, 2642–2649 (2017).
38. A. Chen, Y. Zhao, P. Li, X. Zhang, R. Peng, H. Huang, L. Zou, X. Zheng, S. Zhang, P. Miao, Y. Lu, J. Cai, C. Nan, Angular dependence of exchange bias and magnetization reversal controlled by electric-field-induced competing anisotropies. *Adv. Mater.* **28**, 363–369 (2016).
39. K. Roy, S. Bandyopadhyay, J. Atulasimha, Hybrid spintronics and straintronics: A magnetic technology for ultra low energy computing and signal processing. *Appl. Phys. Lett.* **99**, 063108 (2011).
40. T. Wu, M. Bao, A. Bur, H. K. D. Kim, K. P. Mohanchandra, C. S. Lynch, G. P. Carman, Electrical tuning of metastable dielectric constant of ferroelectric single crystals for low-power electronics. *Appl. Phys. Lett.* **99**, 182903 (2011).
41. H. Cai, W. Kang, Y. Wang, L. Naviner, J. Yang, W. Zhao, High performance MRAM with spin-transfer-torque and voltage-controlled magnetic anisotropy effects. *Appl. Sci.* **7**, 929 (2017).
42. S. Yu, P. Chen, Emerging memory technologies: Recent trends and prospects. *IEEE Solid-State Circuits Mag.* **8**, 43–56 (2016).
43. J. Irwin, S. Lindemann, W. Maeng, J. J. Wang, V. Vaithyanathan, J. M. Hu, L. Q. Chen, D. G. Schlom, C. B. Eom, M. S. Rzchowski, Magnetoelectric coupling by giant piezoelectric tensor design. arXiv:1901.02456 [physics.app-ph] (2019).
44. J.-M. Hu, Z. Li, L.-Q. Chen, C.-W. Nan, High-density magnetoresistive random access memory operating at ultralow voltage at room temperature. *Nat. Commun.* **2**, 553 (2011).
45. H. Wu, Y. Huang, F. Xu, Y. Duan, Z. Yin, Energy harvesters for wearable and stretchable electronics: From flexibility to stretchability. *Adv. Mater.* **28**, 9881–9919 (2016).
46. A. Ben Amar, A. B. Kouki, H. Cao, Power approaches for implantable medical devices. *Sensors* **15**, 28889–28914 (2015).
47. M. Shanthi, L. C. Lim, K. K. Rajan, J. Jin, Complete sets of elastic, dielectric, and piezoelectric properties of flux-grown [011]-poled $Pb(Mg_{1/3}Nb_{2/3})O_3$-(28-32)% $PbTiO_3$ single crystals. *Appl. Phys. Lett.* **92**, 142906 (2008).
48. M. T. Johnson, P. Bloemen, F. DenBroeder, J. J. DeVries, Magnetic anisotropy in metallic multilayers. *Rep. Prog. Phys.* **59**, 1409–1458 (1996).

Acknowledgments: We acknowledge the Nanofabrication Core Lab at King Abdullah University of Science and Technology (KAUST) for excellent assistance. **Funding:** This work was supported by KAUST Office of Sponsored Research (OSR) under award no. CRF-2017-3427-CRG6. P.L. acknowledges support from the National Natural Science Foundation of China (grant no. 11604384) and the State Key Laboratory of Low-Dimensional Quantum Physics (grant no. KF201717). **Author contributions:** A.C. conceived the idea and designed the experiments. X.-X.Z. supervised the project. A.C. performed the magnetic and magnetotransport measurements. Y.Z. and Y.W. deposited MTJ multilayers. A.C. fabricated the devices using photolithography and ion milling. Y.Z. wrote the LabVIEW procedures for magnetotransport measurements. P.L. performed the micromagnetic simulation. L.P. and P.L. performed the finite element simulation. A.C. and X.-X.Z. analyzed the data and wrote the manuscript. All authors read and commented on the manuscript. **Competing interests:** The authors declare that they have no competing interests. **Data and materials availability:** All data needed to evaluate the conclusions in the paper are present in the paper and/or the Supplementary Materials. Additional data related to this paper may be requested from the authors.

Submitted 25 June 2019
Accepted 21 October 2019
Published 13 December 2019
10.1126/sciadv.aay5141

Citation: A. Chen, Y. Zhao, Y. Wen, L. Pan, P. Li, X.-X. Zhang, Full voltage manipulation of the resistance of a magnetic tunnel junction. *Sci. Adv.* **5**, eaay5141 (2019).